Nano-domains segmentation on AFM images

X. Luciani[1], L. Patrone[1] and P. Courmontagne[1]

[1] *L2MP-CNRS UMR 6137, ISEN-Toulon, Maison des Technologies,*
Place G. Pompidou, 83000 Toulon, France

Abstract. The goal of this article is to present a new automatic processing allowing a segmentation of AFM images with the aim of obtaining with precision the dimensions of nano-domains. The proposed treatment is based on the wedding of the multiresolution analysis with a thresholding method. Results obtained on real data are proposed.

1. INTRODUCTION

Size reduction of electronic devices imposes to be able to prepare size-defined nanostructures on a substrate compatible with an industrial process, like silicon. Within the field of molecular electronics [1] a promising solution consists in using molecular self-assembly [2] as a non lithographic method of nanostructuration. In this work, we focused on alkyltrichlorosilane molecules due to their robust grafting on a Si surface covered with its native oxide [2], in order to develop a control of the formation of molecular nano-domains on Si which could serve as a template for grafting active molecules on top of them [3]. Once molecules are self-assembled, Atomic Force Microscopy (AFM) is a suitable tool to analyze the main characteristics like the size, the shape, and the density of nano-domains. The goal of the present work is to obtain automatically, from AFM images, information about the size distribution of nano-domains. After a brief description of the preparation of molecular domains and the nature of AFM images, we present in a second part the multiresolution analysis. Then in the third and last part, we explain the way to obtain precise image segmentation. Each part is largely illustrated with results obtained on real data.

2. NANO-DOMAINS AND AFM IMAGES

Dipping an oxidized silicon substrate in a solution of alkyltrichlorosilanes leads to the transfer of the molecules onto the surface. Below a critical temperature depending on the chain length, molecules are grafted nearly perpendicular to the surface following an island growth [4] up to the complete monolayer formation a few minutes later. Such a growth mode is driven by van der Waals intermolecular interactions during the diffusion of the molecular species on the surface before grafting. It is usually very difficult to monitor the island characteristics such as the shape and size distribution simply by controlling the dipping time. A promising way to improve the nano-domain control is to use a binary mixture of two different molecules "A" and "B" (e.g. molecules of different lengths). This leads to phase separation on the substrate between molecular domains of one molecule and a phase of the other one [5]. However, in order to obtain a model system with very different island sizes allowing analysis of AFM images, we chose to prepare nano-domains of n-octadecyltrichlorosilane (18 carbon atoms, $\sim$25 Å long) by removing the sample from the solution after a few seconds. The solution was prepared at 10^{-2} mol/l in a mixture of hexadecane and carbon tetrachloride (7:3). Then the sample is rinsed using chloroform in an ultrasonic bath and dried with a nitrogen flow. At the end, it is necessary to wipe carefully the surface with a chloroform soaked soft paper to remove the excess of non-grafted molecules. A typical AFM image of the resulting nanostructured surface is shown in figure 1, where nano-domains appear brighter. As it can
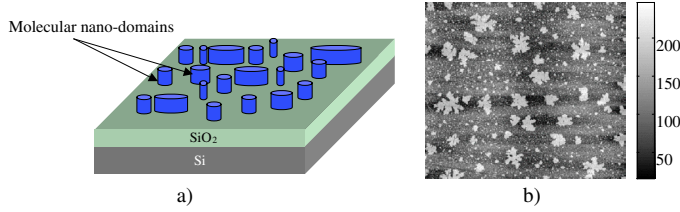
Figure 1. a) 3D representation of molecular nano-domains of different sizes grafted onto Si/SiO$_2$. b) Corresponding typical AFM image of n-octadecyltrichlorosilane domains obtained after a dipping time of a few seconds at T = 20°C. Image size is 7µm × 7µm (512 × 512 pixels). Encoding: 8 bits.

be seen, there are very large differences in molecular island lateral sizes ranging from tens to hundreds of nanometers.

3. MULTIRESOLUTION ANALYSIS

Automatically obtaining, from AFM pictures, information about the size and the distribution of the nano-domains could not be easily achieved because AFM images are highly corrupted by noise. This noise has many origins: procedure (stripes on the surface), acquisition system (roughness, zones of shade, piezoelectric curvature). The signal of interest and the noise being not stationary, we propose to expand the AFM image using a multiresolution analysis: the discrete wavelet transform.

3.1 Multiresolution analysis for a one-dimensional signal

The multiresolution analysis has been first described by Mallat [6]. It results from the embedded subsets generated by the interpolations at different scales.

From the signal $S(t)$ and using the impulse response h of a low-pass filter, we obtain for each studied scale j ($j > 0$) a scaling plane $c_{j+1}[k]$, computed directly from $c_j[k]$:

$$c_{j+1}[k] = \sum_n h[n - 2k]c_j[n]. \qquad (1)$$

Scaling plane $c_0[k]$ corresponds to the response of a filter, described by a scaling function $\phi(t)$, to the signal $S(t)$. This scaling function $\phi(t)$ is linked to the choice of impulse response h. Step by step, because of the nature of h, the signal is smoothed and information is lost. So, the scaling plane $c_j[k]$ represents an approximation of signal $S(t)$ at scale j. The remaining information $w_j[k]$, corresponding to the lost details of $S(t)$, is obtained using the following relation:

$$w_{j+1}[k] = \sum_n g[n - 2k]c_j[n], \qquad (2)$$

where g is of high-pass nature.

The restoration is performed using two conjugated filters $\tilde{h}$ and $\tilde{g}$ to h and g:

$$c_j[k] = 2 \sum_n (c_{j+1}[n]\tilde{h}[k + 2n] + w_{j+1}[n]\tilde{g}[k + 2n]). \qquad (3)$$

3.2 The *à Trous* algorithm for one-dimensional signal

The *à Trous* algorithm is a discrete wavelet decomposition algorithm, developed by Holdschneider [7]. It is conform to the multiresolution analysis defined by Mallat.

Denoting $\delta[k]$ the Kronecker symbol, this algorithm sets the following relation between h and g:

$$g[k] = \delta[k] - h[k]. \tag{4}$$

From this relation, wavelet coefficients $w_j[k]$ become:

$$w_j[k] = c_{j-1}[k] - c_j[k]. \tag{5}$$

Consequently, the two filters $\tilde{h}$ and $\tilde{g}$ are such as $\tilde{h}[k] = \tilde{g}[k] = 1$, so that signal at scale 0, $c_0[k]$, can be exactly reconstructed by summing all the wavelet planes together with the smoothed data $c_q[k]$:

$$c_0[k] = c_q[k] + \sum_{j=1}^{q} w_j[k]. \tag{6}$$

For each scale j, the wavelet plane w_j is computed. The number of coefficients for each wavelet plane is the same (there is no down-sampling). So for each point k, the corresponding wavelet coefficient at each scale is known, which is perfectly adapted to precise image segmentation.

3.3 Implementation and denoising step

We can find in the literature several scaling functions. The interpolation of the third order B-splines introduced by [8] allows very high performances. It defines the continuous 1D form of the B-Spline scaling function:

$$\phi(t) = (|t - 2|^3 - 4|t - 1|^3 + 6|t|^3 - 4|t + 1|^3 + |t + 2|^3)/12 \tag{7}$$

The filter h associated with $\phi(t)$ is equal to $(1, 4, 6, 4, 1)/16$. Filter h_{2D} for an image is determined using the variable separation for the two-dimensional scaling function: $h_{2D} = {}^t h \otimes h$.

If the image I to analyze is quite regular, the c_0 coefficients can be considered equal to I. The figure 2 represents the *à Trous* wavelet transform of the studied AFM picture. For this experiment, the c_0 values are approximated to the original image, the c_j values (for j greater than 0) are computed by applying the h_{2D} low-pass filter on the c_{j-1} values and the w_j values are obtained by taking the difference between c_{j-1} and c_j.
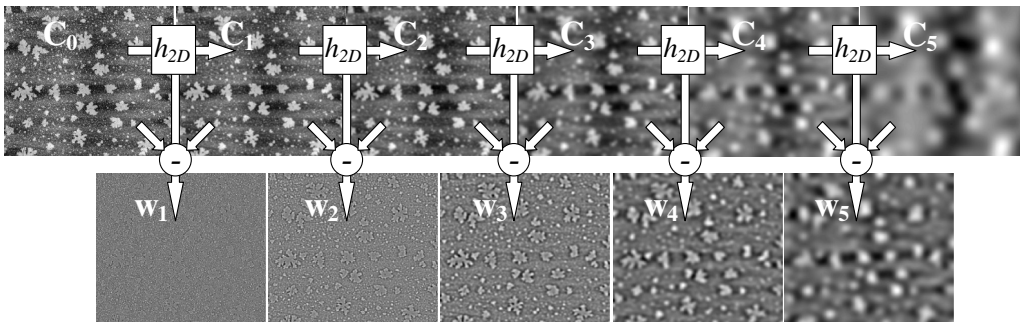

Figure 2. The *à Trous* wavelet transform of the studied AFM picture.

An analysis of this figure shows the repartition of the noise in the different planes: the strips on the surface and the roughness are mainly present in w_1, the zones of shade in w_5 and the piezoelectric curvature in c_5. For this reason, a denoising step of this AFM picture can be made by keeping only the w_2, w_3 and w_4 components ($\hat{I} = w_2 + w_3 + w_4$). This way, we obtain the filtered image $\hat{I}$ proposed in figure 3.a.

4. THRESHOLDING AND IMAGE LABELLING

As we can see in figure 3.a, we still need to extract the nano-domains from the background. Thanks to the multiresolution analysis described in the previous part, the nano-domains in figure 3.a present a high signal to noise ratio. Consequently, we can assume that an appropriate thresholding method will be enough. The better results (presented in figure 3.b) were obtained with a method presented by Otsu [9], consisting in maximizing the inter-class variance, defined by relation (8). We separate the grey scaled image into two different classes $C_1(k)$ and $C_2(k)$ containing all the pixels having a grey level above or under the value k, respectively. The aim is to find the threshold η, which ensures that $C_1(\eta)$ will only contain the signal (nano-domains) and $C_2(\eta)$ will only contain background pixels.

$$\sigma_B^2(k) = P(C_1(k)) \times (M_1(k) - M)^2 + P(C_2(k)) \times (M_2(k) - M)^2, \tag{8}$$

where $P(C_i(k))$ is the probability that a pixel belongs to $C_i(k)$, $M_i(k)$ is the mean value of $C_i(k)$ and M is the mean value of the entire image. Thus, the best threshold η will be:

$$\eta = \arg\max_k \left\{ \sigma_B^2(k) \right\}. \tag{9}$$

The last step of our process is the image labelling. We used a relatively simple algorithm, consisting in replacing the value of each pixel of a particular nano-domain i by the same value k_i. The only constraint is that k_i must be different than k_j for $i \neq j$. For that, we substitute all the N pixels different from 0 of the image by N different integers. Then, each pixel, different from 0, is replaced by the smallest value (different from 0) of its vicinity. Then, we just have to count the number of pixels having a value equal to k_i, to convert it into μm^2, using the resolution used by the AFM, to know the area of the nano-domain and replace the particular value k_i of each nano-domain by the value of its area. The result is presented in figure 3.c.
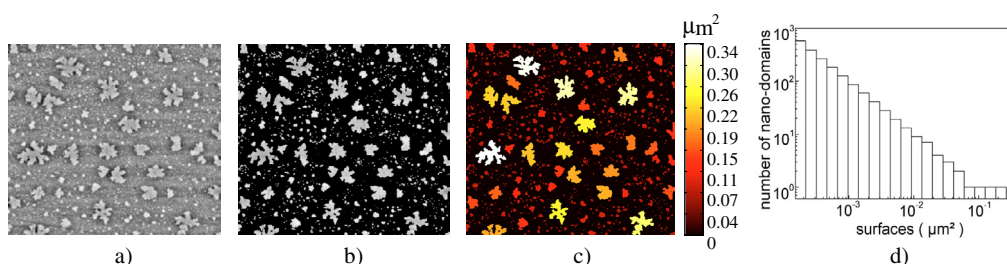

Figure 3. a) Filtered AFM picture, b) Filtered AFM picture after thresholding, c) Image labelling 7μm × 7μm, d) Size distribution in logarithmic scales.

An analysis of these results shows that the denoising step allows a good reduction of the noise. Indeed, the piezoelectric curvature has disappeared, there are no more zones of shade and the roughness amplitude was clearly decreased compared to that of the nano-domains. Furthermore, the largest nano-domain in left-bottom of the image, presented in figure 1.b, was cut into two by a stripe, which is not any more the case on the final image (figure 3.c). Using such a processing, from AFM images, we are able to determine automatically some physical parameters of nano-domains, such as surfaces (between 2.10^{-4} μm^2 and $0.38\,\mu m^2$ for this image), size distribution (figure 3.d) or coverage (near 20% for the current image), which is quite impossible using the original image. One can see in figure 3.d that the obtained distribution of nano-domain areas (denoted as A in the following) exhibits typical power-law behaviour in $\sim A^{-1}$ [10]. Such a power-law means that coverage is equal for each domain size. This is consistent with the expected continuous nucleation-aggregation process supplied by a constant adsorption rate of molecules from solution to substrate, thus validating the applied image processing.

5. CONCLUSION

We have presented an automatic data processing sequence allowing a segmentation of AFM images of self-assembled molecules with the aim of obtaining with precision the surface of nano-domains. Results obtained on real data reveal the effectiveness of the proposed treatment. A systematic use of this process allows a precise analysis of the growth characteristics of such molecular systems.

References

[1]   C. Joachim, J.K. Gimzewski, A. Aviram, *Electronics using Hybrid-Molecular and Mono-Molecular Devices*, Nature 408 (2000), pp.541-548.

[2]   F. Schreiber, *Structure and Growth of Self-Assembling Monolayers*, Progress in Surf. Sci. 65 (2000), pp.151-256.

[3]   S. Lenfant, C. Krzeminski, C. Delerue, G. Allan, D. Vuillaume, *Molecular Rectifying Diodes from Self-Assembly on Silicon*, Nano Lett. 3 (2003), pp.741-746.

[4]   C. Carraro, O.W. Yauw, M.M. Sung, R. Maboudian, *Observation of Three Growth Mechanisms in Self-Assembled Monolayers*, J. Phys. Chem. B 102 (1998), pp.4441-4445.

[5]   B.L. Kropman, D.H.A. Blank, H. Rogalla, *Binary Mixtures of Self-Assembled Monolayers on $SrTiO_3$: Experimental Evidence for Phase Segregation,* Langmuir 16 (2000), pp.1469-1472.

[6]   S. Mallat, *A Theory for Multiresolution Signal Decomposition: The Wavelet Representation*, Proc. IEEE Trans on Pattern Anal. and Math. intel., Vol. 11 (1989), No 7, pp.674-693.

[7]   M. Holdschneider, R. Kronland-Martinet, J. Morlet, P. Tchamitchian, *A real time algorithm for the Signal Analysis with the help of the wavelet transform*, in *Wavelets*. ed. J.M. Combes et al. Springer-Verlag Berlin (1989), pp.286-297.

[8]   M. Unser, A. Aldroudi, *Polynomial Splines and Wavelets - A Signal Processing Perspective*, in *Wavelets: A Tutorial in Theory and Applications*, ed. C.K.Chui Academic Press New York (1992), pp.91-122.

[9]   N. Otsu. *A Threshold Selection Method from Gray-level Histograms*, IEEE Trans. Syst. Man & Cybern., Vol.SMC-9 (1979), No.1, pp.62-66.

[10] S. Desbief, Ph.D. Thesis, University of Provence, Marseille, France (2005).